

# Cosmic Ray particle production

J. Ranft<sup>a\*</sup>

<sup>a</sup>INFN, Lab. Naz. del Gran Sasso, I-67010 Assergi, Italy

The status of some popular models to simulate hadronic and nuclear interactions at Cosmic Ray energies is reviewed. The models predict the rise of all the hadronic and nuclear cross sections with energy and a smooth (logarithmic) rise of average multiplicities, rapidity plateaus and average transverse momenta with the energy. Big differences are found between model predictions partly already at energies, where collider data are available. It is argued, that at the highest energies data of the Cosmic Ray cascade can only be reliably interpreted by sampling the cascade using more than one model. The importance is stressed to put more effort into the models and especially a better understanding of the minijet component at the highest energies. Likewise, experimental data on particle production are needed at the highest possible energies, to guide the models.

*Presented at the International Symposium on Multiparticle Dynamics Frascati, Italy Sept. 8 to 12 1997*

## 1. Introduction

The extension of models for multiparticle production in hadron-hadron, hadron-nucleus and nucleus-nucleus collisions to be used for the simulation of the Cosmic Ray cascade up to  $E_{lab} = 10^{21}$  eV (corresponding to  $\sqrt{s} = 2000$  TeV) is needed to prepare for the Auger experiment [1] as well as for a reliable interpretation of present experiments like Agasa [2] and Flys Eye [3], which present data in the EeV energy region. The need for careful comparisons of hadron production models was stressed at the International Cosmic Ray Conference in Roma 1995. Following this, such a code comparison in the energy region of interest to the Kaskade experiment [4] was presented by members of the Kaskade experiment [5]. From this code comparison it became clear, that already in the knee region of the Cosmic Ray energy spectrum important differences exist between the models and that these differences might change the interpretation of certain Cosmic Ray results. Here we will discuss the status of some of these models, discuss the minijet component, present typical comparisons to Collider data, present some characteristics of hadron production up to  $E_{lab} = 10^{21}$  eV and finally compare some results obtained simulating the cosmic

ray cascade using different models.

## 2. The present status of some event generators used for Cosmic Ray cascade simulations

The presently dominant hadron production models used for the simulation of the Cosmic Ray cascade are constructed on the basis of multi-string fragmentation, they use Gribov-Regge and Gribov-Glauber theory, to construct the multi-string production in hadron-hadron and nuclear collisions. Most of the models use minijets as an important mechanism for particle production at high energies.

The DPMJET-II event generator based on the two-component Dual Parton Model (DPM) was described in detail [6-8]. The extension of this model up to energies of  $\sqrt{s} = 2000$  TeV was reported this year, the resulting model will be referred to as DPMJET-II.3. The extension is done by calculating the minijet component of the model using new parton distribution functions, the GRV-LO parton distributions [9] and the CTEQ4 parton distributions [10], which are both available in a larger Bjorken- $x$  range than the MRS(D-) parton distributions, which were the default in DPMJET-II.2. These new parton distributions describe the structure function data measured in the last years at the HERA Collider. DPMJET-II.3 describes well minimum bias

\*Present address: FIGS and Physics Dept. Universität Siegen, D-57068 Siegen Germany, e-mail: Johannes.Ranft@cern.ch

hadron and hadron jet production up to present collider energies. It is also demonstrated, that the model performs as well as the previous one DPMJET-II.2 for hadron production in hadron-nucleus and nucleus-nucleus collisions. DPMJET is used for the simulation of the Cosmic Ray cascade within the HEMAS-DPM code [11] used mainly for the MACRO experiment [12].

The SIBYLL model [13] is a minijet model and has been reported to be applicable up to  $E_{lab} = 10^{20}$  eV. However, the EHQL [14] parton structure functions used for the calculation of the minijet component might, after the HERA experiments, no longer be adequate. It is known, that a significant updating of SIBYLL is planned for the next year. SIBYLL is the most popular model for simulating the Cosmic Ray cascade in the USA.

VENUS, a very popular model applied originally for describing heavy ion experiments, is now the leading event generator within the Corsika Cosmic Ray cascade code [15]. VENUS is applicable up to  $E_{lab} = 5 \times 10^{16}$  eV. It has been reported [16], that the introduction of minijets into VENUS has been planned, this will allow to apply VENUS up to higher energies.

QGSJET [17] is the most popular Russian event generator used for Cosmic Ray simulations. It is based on the Quark Gluon String (QGS) model, this model is largely equivalent to the DPM. QGSJET also contains a minijet component and is reported to be applicable up to  $E_{lab} = 10^{20}$  eV.

HPDM [18] is based on parametrizations inspired by the DUAL Parton Model. it is reported to be applicable up to  $E_{lab} = 10^{20}$  eV, however some of the parametrizations might become unreliable above  $E_{lab} = 10^{17}$  eV. HPDM was originally used as event generator within the Corsika cascade code.

MOCCA [19] is an empirical model employing a successive splitting algorithm. It was reported to be applicable up to  $E_{lab} = 10^{20}$  eV. Since the model does not contain minijets, its predictions at the upper energy end might differ significantly from the other models.

In Table 1 we present some characteristics of the models. The Gribov-Regge theory is applied by three of the models. The pomeron intercept

for SIBYLL is equal to one, SIBYLL is a minijet model using a critical pomeron, with one soft chain pair, all the rise of the cross section results from the minijets. In the models with pomeron intercept bigger than one, we have also multiple soft chain pairs, already the soft pomeron leads to some rise of the cross sections with energy. Minijets are used in three of the models, it is believed, that minijets are necessary to reach the highest energies. All models contain diffractive events. Secondary interactions between all produced hadrons and spectators exist only in VENUS, DPMJET has only a formation zone intranuclear cascade (FZIC) between the produced hadrons and the spectators. Only three of the models sample properly nucleus-nucleus collisions, the other two models replace this by the superposition model, where the nucleus-nucleus collision is replaced by some hadron-nucleus collisions. The residual projectile (and target) nuclei are only given by two of the models.

**Table 1.** Characteristics of some popular models for hadron production in Cosmic Ray cascades. (VEN = VENUS, QGS = QGSJET, SIB = SIBYLL, HP = HPDM, DPM = DPMJET)

	VEN	QGS	SIB	HP	DPM
Grib.-Regg.	x	x			x
Pom. ic.	1.07	1.07	1.00		1.05
minijets		x	x		x
Diffr. ev.	x	x	x	x	x
sec. int.	x				x
A-A int.	x	x			x
superp.			x	x	
res. nucl.		x			x
max. E [GeV]	$10^7$	$10^{11}$	$10^{11}$	$10^8$	$10^{12}$

### 3. The calculation of the minijet component

The input cross section (before the unitarization procedure applied by the models) for semi-hard multiparticle production (or minijet production)  $\sigma_h$  is calculated applying the QCD improved parton model, the details (for DPMJET) are given in Ref.[20–25].

$$\sigma_h = \sum_{i,j} \int_0^1 dx_1 \int_0^1 dx_2 \int d\hat{t} \frac{1}{1 + \delta_{ij}} \frac{d\sigma_{QCD,ij}}{d\hat{t}} \times f_i(x_1, Q^2) f_j(x_2, Q^2) \Theta(p_{\perp} - p_{\perp thr}) \quad (1)$$

$f_i(x, Q^2)$  are the structure functions of partons with the flavor  $i$  and scale  $Q^2$  and the sum  $i, j$  runs over all possible flavors. To remain in the region where perturbation theory is valid, a low  $p_{\perp}$  cut-off  $p_{\perp thr}$  is used for the minijet component. Since the HERA measurements, the structure functions are known to behave at small  $x$  like  $1/x^{\alpha}$  with  $\alpha$  between 1.35 and 1.5. The minijet production is dominated by very small  $x$  values, therefore the minijet cross section calculated with the new structure functions rise very steeply with energy. We found already 1993 [25] with the MRS[D-] structure function [26] at the LHC energy a minijetcross section about 10 times larger than the total cross section at this energy.

Such large minijet cross sections are inconsistent and wrong: The input minijet cross sections  $\sigma_h$ , which one puts into the unitarization scheme are inclusive cross sections normalized to  $n_{minijets}\sigma_{inel}$ , where  $n_{minijets}$  is the multiplicity of minijets. The physical processes, which contribute to this inclusive cross section are  $2 \rightarrow n$  parton processes.  $2 \rightarrow n$  processes give a contribution to  $\sigma_h$  equal to  $n\sigma_{2 \rightarrow n}$ . If one treats this huge cross section as  $\sigma_h$  in the usual way in the eikonal unitarization scheme one replaces it by  $n/2$  simultaneous  $2 \rightarrow 2$  parton processes, this is the inconsistency. What one should really use in the unitarization, but what we do not know how to compute reliably at present would be  $\sigma_h = \sum_n \sigma_{2 \rightarrow n}$ . The way to remove this inconsistency is to make in the two component DPM the threshold for minijet production  $p_{\perp thr}$  energy dependent in such a way, that at no energy and

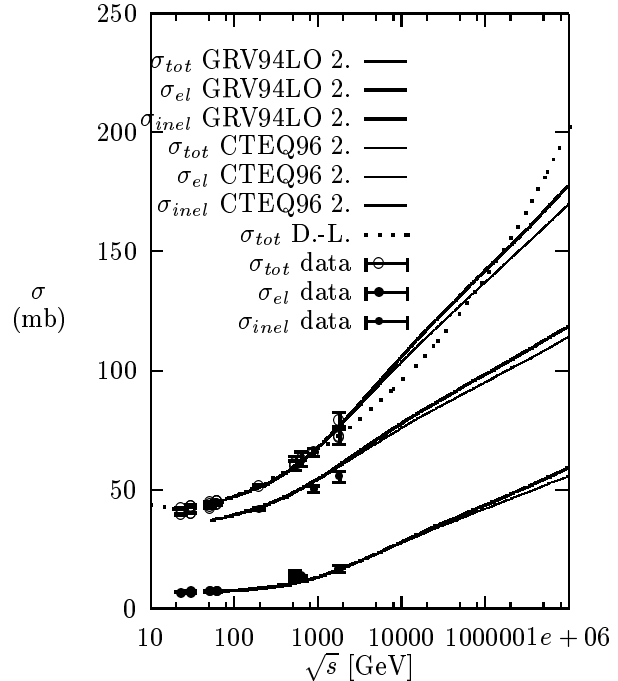


Figure 1. Total, inelastic and elastic  $p\bar{p}$  and  $pp$  cross sections from DPMJET-II.3 as function of the center of mass energy  $\sqrt{s}$ . The model results obtained using the GRV-LO parton distributions [9] and the CTEQ4 parton distributions [10] are compared to the Donnachie–Landshoff fit for the total cross section [27] and to data [28–30] [31–36]

for no PDF the resulting  $\sigma_h$  is much bigger than the total cross section. Then at least we have a cross section, which is indeed mainly the cross section of a  $2 \rightarrow 2$  parton process at this level, the parton–parton scattering with the largest transverse momentum. We can get back to the real  $2 \rightarrow n$  processes and recover the minijets with smaller transverse momenta via parton showering. One possible form for this energy dependent cut off is [25]:

$$p_{\perp thr} = 2.5 + 0.12[\lg_{10}(\sqrt{s}/\sqrt{s_0})]^3 \quad (2)$$

[GeV/c],  $\sqrt{s_0} = 50\text{GeV}$ .

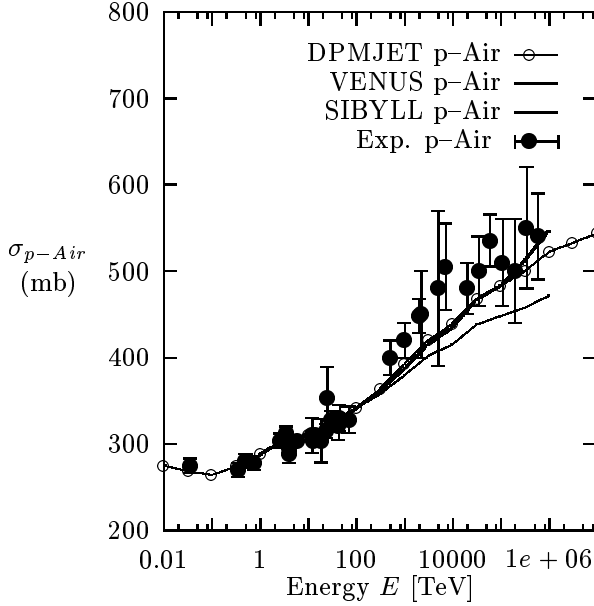


Figure 2. The inelastic cross section  $\sigma_{p-Air}$  calculated by DPMJET-II.3 (as well as the ones from VENUS and SIBYLL according to Ref. [5]) as function of the laboratory collision energy (from 0.02 TeV up to 1.E9 TeV) compared to experimental data collected by Mielke et al. [37].

The resulting  $\sigma_h$  are smaller or not much larger than the total cross sections resulting after the unitarization for all PDF's.

There are further features of the minijet component worth mentioning. One uses as first described in [24] at  $p_{\perp thr}$  the continuity requirement for the *soft* and *hard* chain end  $p_{\perp}$  distributions. Physically, this means, that we use the soft cross section to cut the singularity in the minijet  $p_{\perp}$  distribution. But note, that this cut moves with rising collision energy to higher and higher  $p_{\perp}$  values. This procedure has besides cutting the singularity more attractive features:

(i) The model results (at least as long as we do not violate the consistency requirement described above) become somewhat independent from the otherwise arbitrary  $p_{\perp}$  cut-off. This was already

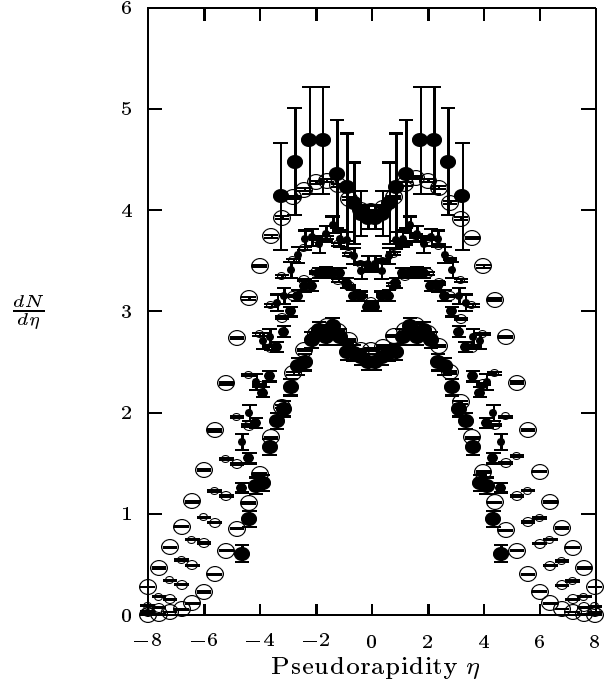


Figure 3. Pseudorapidity distributions of charged hadrons produced in nondiffractive  $p\bar{p}$  collisions at  $\sqrt{s} = 0.2, 0.54, 0.9$  and  $1.8$  TeV. The DPMJET-II.3 results are compared with data from the UA-5 Collaboration [38] and from the CDF Collaboration [39].

demonstrated with DTUJET90 [22] and cut-offs of 2 and 3 GeV/c.

(ii) The continuity between soft and semihard physics is emphasized, there is no basic difference between soft and semihard chains besides the technical problem, that perturbative QCD allows only to calculate the semihard component.

(iii) With this continuity in mind we feel free to call all chain ends, whatever their origin in the model, minijets, as soon as their  $p_{\perp}$  exceeds a certain value, say 2 GeV/c.

#### 4. Comparing the models to data at accelerator and collider energies

Each model has to determine its free parameters. This can be done by a global fit to all available data of total, elastic, inelastic, and single diffractive cross sections in the energy range from ISR to collider experiments as well as to the data on the elastic slopes in this energy range. Since there are some differences in the hard parton distribution functions at small  $x$  values resulting in different hard input cross sections we have to perform separate fits for each set of parton distribution functions. After this stage each model predicts the cross sections also outside the energy range, where data are available. In Fig. 1 we plot for DPMJET-II.3 the fitted cross sections obtained with two PDF's together with the data. Furthermore we compare the total cross sections obtained with the popular Donnachie–Landshoff fit [27]. For applications in Cosmic Ray cascade simulations we need in particular the hadron–Air cross section. In Fig.2 we compare data according to Mielke et al. [37] with the cross sections according to three models. At low energies all models are describing these data rather well. At high energies we observe however small differences between the models.

At higher energies (and in non-single diffractive  $p\bar{p}$  collisions) there are pseudorapidity distributions from the UA–5 Collaboration [38] and from the CDF Collaboration [39]. In Fig.3 a very good agreement is found of DMJET-II.3 with these data. Still very often there is and was always (see Fig.3) a disagreement of the models with the UA–5 data at the highest pseudorapidity values. The models predict systematically more particles at the largest pseudorapidities of the experiment. This disagreement (if the data would be correct) would of course be of importance, if one is interested in Cosmic Ray cascades, where the particle production in the fragmentation region is of main interest. Fortunately, a new independent measurement of the pseudorapidity distribution in the collider energy range became available recently [40]. In Fig. 4 the comparison with this new data is presented and we find a remarkable agreement with DPMJET-II.3 in the large pseudorapidity

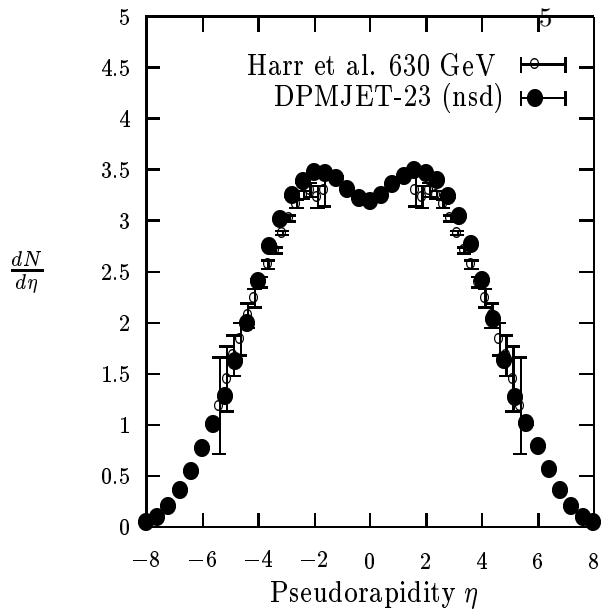


Figure 4. Pseudorapidity distributions of charged hadrons produced in nondiffractive  $p\bar{p}$  collisions at  $\sqrt{s} = 0.63$  TeV. The DPMJET-II.3 results are compared with recent data from Harr et al. [40]. [41].

region. In Fig.5 we present the comparison (from Ref.[5]) of multiplicity distributions according to 5 models with the data from the UA–5 Collaboration [38]. Most of the models describe at least the high multiplicity tail of the data reasonably well, however the multiplicity distribution according to the SIBYLL model is everywhere rather far from the data. We turn to collisions with nuclei. In Fig. 6 the comparison of DPMJET-II.3 is with the rapidity distribution of charged hadrons in p–Ar collisions at 200 GeV. In Fig. 6 we compare with the rapidity distribution of negatively charged hadrons in central S–S and S–Ag collisions.

At least in models with a minijet component we expect good agreement with data on transverse momentum distributions. In Fig.8 we compare hadron jet production in DPMJET-II.3 with data from the CDF–Collaboration [44]. The jets from the model are found out of the Monte Carlo events using a jet finding algorithm with the same

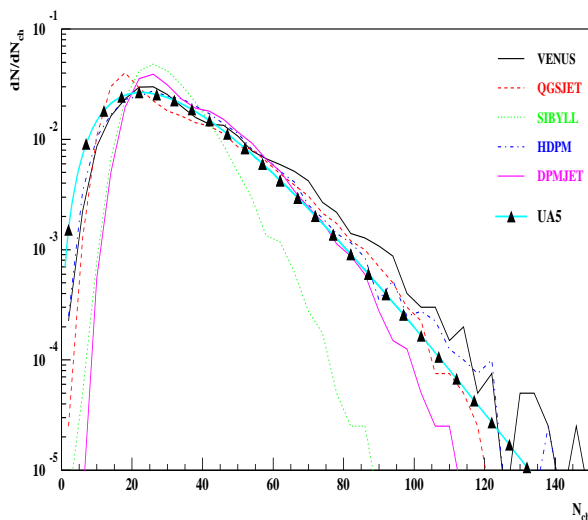


Figure 5. Multiplicity distribution of charged hadrons from nondiffractive  $\bar{p}-p$  collisions at  $\sqrt{s} = 540$  GeV. The data are from the UA-5 Collaboration [38]. The comparison with 5 models is from [5].

parameters like the one used by the experiment. With a minimum bias Monte Carlo event generator it is of course not possible to obtain good statistics on the total transverse energy range of the experiment. We find good agreement of the jets in the model with the data up to  $E_{\perp} = 30$  GeV/c. The transverse momentum distribution in a large  $p_{\perp}$  region was determined by the UA-1-MIMI Collaboration [45]. In Fig.9 we compare DPMJET-II.3 results with the parametrization of the data given by this experiment and we find a good agreement.

In Fig.10 we compare average transverse momenta as obtained from DPMJET-II.3, QGSJET and SIBYLL as function of the cms energy  $\sqrt{s}$  with data collected by the UA-1 Collaboration. This plot gives at the same time the DPMJET predictions for the average transverse momenta up to  $\sqrt{s} = 2000$  TeV and the predictions of the two other models up to  $\sqrt{s} = 100$  TeV. While at energies where data exist all models agree rather well with each other and with the data, we find

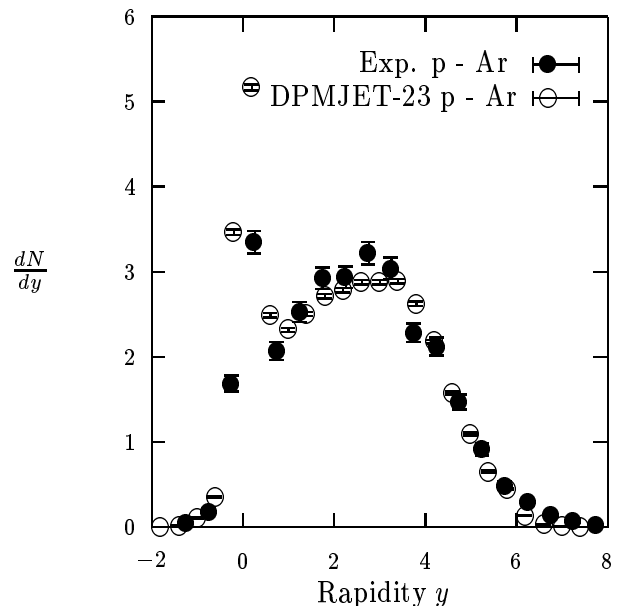


Figure 6. Charged particle rapidity distribution for p-Ar interactions. The DPMJET-II.3 results are compared with data [42].

completely different extrapolations to higher energies. We should note, this are just the three models with a minijet component. But it seems, that in spite of the minijets the average transverse momentum in QGSJET becomes constant at high energies, while it continues to rise in DPMJET. For me the rise of the average transverse momentum in DPMJET is connected with the fact, that with the new parton structure functions since the HERA measurements really the minijets dominate very much all of hadron production at high energy. We can conclude, there are very big differences in implementing the minijet components in the models.

## 5. Properties of the models in the highest energy region

In Fig.11 the pseudorapidity distributions for charged hadrons according to DPMJET-II.3 are presented for energies between  $\sqrt{s} = 1$  TeV and 2000 TeV. The width of the distributions increases like the logarithm of the energy and also

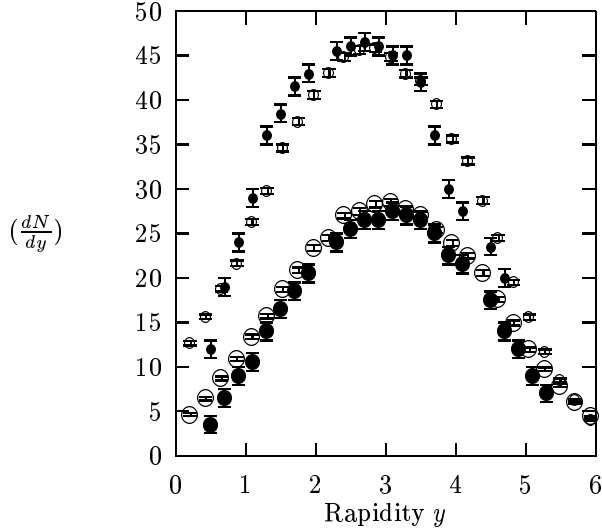


Figure 7. Rapidity distribution of negatively charged hadrons in central S-S and S-Ag collisions. The results of DPMJET-II.3 are compared with data from the NA-35 Collaboration [43].

the maximum of the curves rises like the logarithm of the energy. If we call the central region around the two maxima the plateau, then we find the width of this plateau hardly to change with energy. Fig.12 presents the rise of the total charged multiplicity with the cms energy  $\sqrt{s}$  according to DPMJET, QGSJET and SIBYLL. we find again, at low energies, where data are available, the models agree rather well. DPMJET and SIBYLL agree in all the energy range shown. However, QGSJET above the energy of the TEVATRON extrapolates to higher energies in a completely different way.

In Fig.13 we present for  $pp$  and  $p$ -Air collisions the energy fractions  $K$  for  $B - \bar{B}$  (baryon - antibaryon) and charged pion production. The cosmic ray spectrum-weighted moments in  $p$ -A collisions are defined as moments of the  $F(x_{lab})$  :

$$Z_i^{p-A} = \int_0^1 (x_{lab})^{\gamma-1} F_i^{p-A}(x_{lab}) dx_{lab} \quad (3)$$

Here  $-\gamma \simeq -1.7$  is the power of the integral cos-

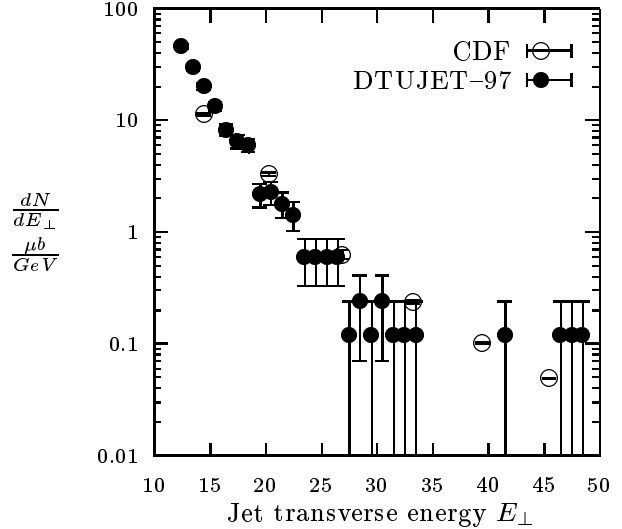


Figure 8. The jet transverse energy distribution is compared with data from the CDF-Collaboration [44]. The jets are found from the model events in the pseudorapidity region  $|\eta| \leq 0.7$  using a jet finding algorithm.

mic ray energy spectrum and  $A$  represents both the target nucleus name and its mass number. In Fig.14 we present the spectrum weighted moments for pion production in  $pp$  and  $p$ -Air collisions as function of the cms energy  $\sqrt{s}$  per nucleon. We find all average values characterizing hadron production: the cross sections (Fig.1), the average transverse momenta (Fig.10) the charged multiplicities (Fig.12), and the moments in Figs. 14 and in Fig. 13 to change smoothly with energy in most cases just like the logarithm of the energy.

### Comparison of the models after simulating the Cosmic Ray cascade

First we present results of a comparison between the cascade code HEMAS [47] using DPMJET as event generator and the cascade code CORSIKA [15] using VENUS as event generator [48]. This comparison has been done for quan-

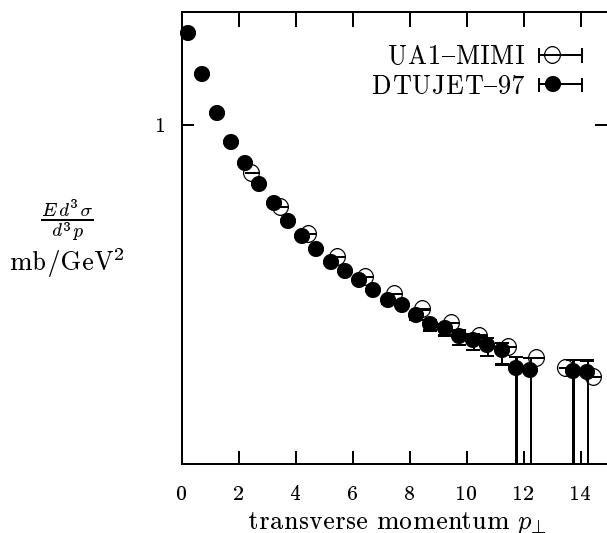


Figure 9. Comparison of transverse momentum cross sections according to DPMJET-II.3 at  $\sqrt{s} = 0.63$  TeV with collider data from the UA-1 MIMI Collaboration [45]. The experimental data are represented by the parametrization given by the Experiment.

tities of interest for the EAS-Top and MACRO experiments in the Gran Sasso Lab. The zenith angle is fixed at 31 degrees (MACRO/EAS-TOP coincidence direction). The e.m. shower size and muons above 1 TeV are sampled at 2000 meters a.s.l. (946 g/cm<sup>2</sup> slant depth, 810 g/cm<sup>2</sup> vert. depth). The calculations were done for primary protons, He nuclei and Fe nuclei with energies between 3 and 2000 TeV. Calculated are for each primary energy and particle (i) the e.m. shower profile, (ii) the Log(e.m. size) at EAS-TOP sampling depth (946 g/cm<sup>2</sup>), (iii) the distance muon-shower axis for  $E > 1$  TeV muons, (iv) the muon decoherence for  $E > 1$  TeV muons, (v) the number of muons per shower and (vi) the energy spectrum of  $E > 1$  TeV muons. In Figs. 15 to 18 we present two of these comparisons. A satisfactory agreement is found in these plots as well as in all other comparisons at different energies and with the other primary particles. Next we

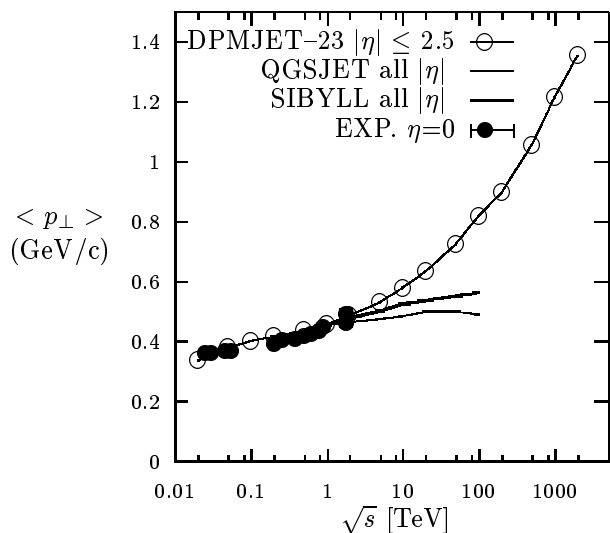


Figure 10. Average transverse momenta of charged secondaries produced in  $p\bar{p}$  and  $pp$  collisions calculated from DPMJET, QGSJET and SIBYLL (The latter two as given in Ref.[5]) as function of the center of mass energy  $\sqrt{s}$  compared to data collected by the UA-1 Collaboration [46].

present two comparisons from the Karlsruhe code comparison [5]. The distributions chosen in this comparison are motivated by the interest of the KASCADE[4] experiment in Karlsruhe. In Fig.19 the Muon multiplicity distribution at ground level is calculated for primary protons of  $E = 10^{15}$  eV. The calculation is done with the CORSIKA cascade code using 5 different event generators for the hadronic interactions. While again VENUS and DPMJET give distributions, which agree very well, it is found, that SIBYLL gives a very different distribution centered at smaller Muon number.

In Figs. 20 and 21 ( The distributions were calculated using the CORSIKA shower code [5] with 5 different event generators for the hadronic interactions. ) Fe and p induced showers with energies of  $E = 10^{14}$  and  $10^{15}$  eV are plotted in the  $\log_{10} N_{\mu} - \log_{10} N_e$  plane (Muon-number



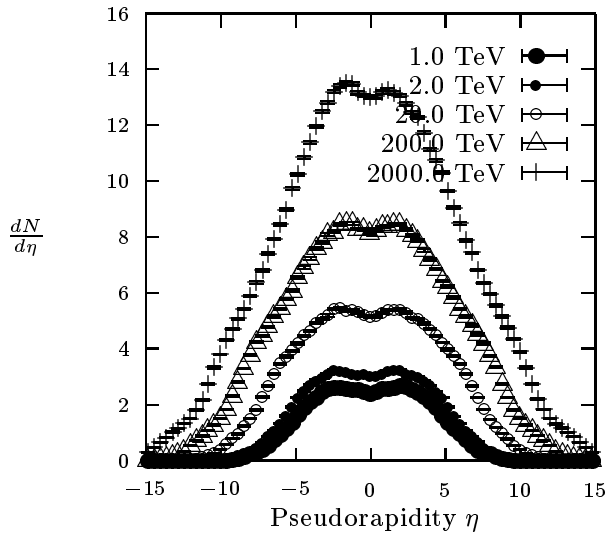


Figure 11. The development of the pseudorapidity distribution of charged hadrons produced in inelastic  $pp$  collisions in the center of mass energy range between  $\sqrt{s}=1$  TeV and  $\sqrt{s} = 2000$  TeV.

-Electron-number plane). The distribution of events according to each of the 5 interaction models for each energy and primary particle is indicated by contours. Considering these plots calculated with only one of the models, where Muon number is plotted over electron number, the impression is, that a simultaneous measurement of Muon-number and Electron number allows to determine the primary energy as well as the composition of the primary component. In these plots we see, that for instance VENUS and DPMJET agree very well, but the contour according to SIBYLL for Fe projectiles of  $E = 10^{15}$  eV overlaps the VENUS and DPMJET contours for p projectiles. From these differences between the models one can conclude, that at present the systematic errors of the cascade calculations (and this are just the differences obtained using different models) prevent to identify safely the composition of the primary component from such measurements.

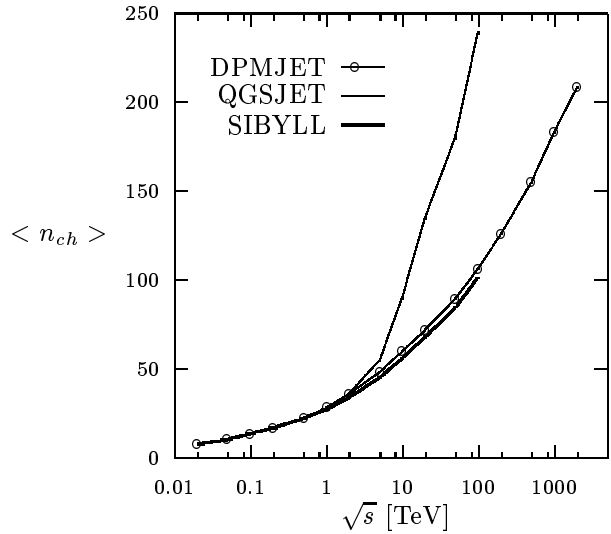


Figure 12. Rise of the charged multiplicity in inelastic  $pp$  collisions according to DPMJET-II.3 in the center of mass energy range between  $\sqrt{s}=0.02$  TeV and  $\sqrt{s} = 2000$  TeV. At energies between 1 and 100 TeV we plot also the average multiplicities according to SIBYLL and QGSJET as given in Ref.[5].

## 6. Conclusions

I would like to stress, more efforts are needed to extend the models used to simulate the hadronic interactions in the C.R. cascade up to the energies to be explored by the Auger Experiment.

At least at collider energies, where data are available, these models should agree among themselves and with the data. Disagreements to data like the ones seen in Fig.5 should be removed as soon as discovered.

A much better understanding is needed how to calculate the minijet component. Certainly, the parton structure functions used for calculating the minijet cross sections should correspond to the HERA measurements at small  $x$ . But this is certainly not the only problem. The differences in the extrapolation to higher energies of quantities like average transverse momenta and charged

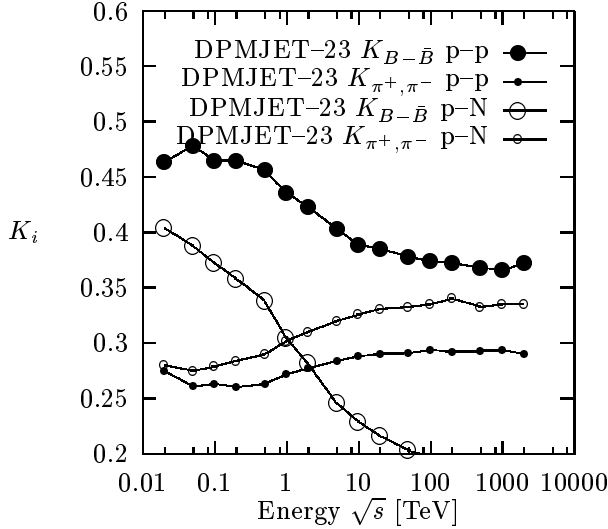


Figure 13. Laboratory energy fractions for  $B-\bar{B}$  and pion production in  $pp$  and  $p$ -Air collisions according to DPMJET-II.3 as function of the (nucleon-nucleon) cms energy  $\sqrt{s}$ .

multiplicities (see Figs. 10 and 12) in the three models implementing minijets are huge. These differences indicate, that much effort is needed to get a better understanding of the minijet component.

Another question, where models disagree is the presence at high energy of an important soft component of hadron production like in the models with a supercritical pomeron. In minijet models all rise of the cross sections and of particle production at high energy is only due to the minijets.

There are (even at energies, where collider data are available, see Fig. 19) large differences between the models after simulating the C.R. cascade. We have to interpret these differences as the systematic errors of the cascade simulation. Such large differences could well prevent the interpretation of otherwise very interesting Cosmic Ray data. In future, C.R. results should always be interpreted using simulations with some different models.

It might be dangerous, that at present many of

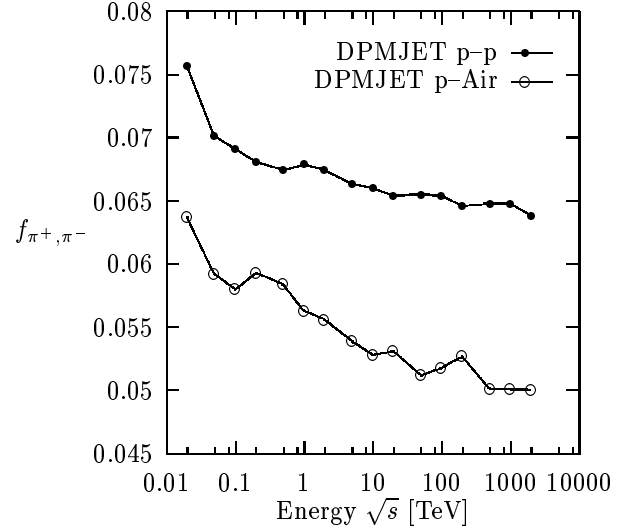


Figure 14. Spectrum weighted moments for pion production in  $pp$  and  $p$ -Air collisions as function of the (nucleon-nucleon) cms energy  $\sqrt{s}$ .

the popular models are based on the same theoretical foundations (and yet might differ very much in their results). To be on the safe side, it would be useful to construct models based also on widely different theoretical concepts (for instance on the string fusion model [49]).

Finally, I would like to stress the need for new measurements of hadron production especially at the highest possible energies. In particular in the fragmentation region so important for the cosmic ray cascade, data (like Feynman- $x$  distributions) from the TEVATRON collider would be highly welcome.

#### Acknowledgements

Thanks are due to J.Knapp, for providing me with some of the Figures from the Karlsruhe code comparison and due to C.Forti for providing me with the Figures from the 2000 TeV code comparison.

#### REFERENCES

1. The Auger Collaboration: Pierre Auger

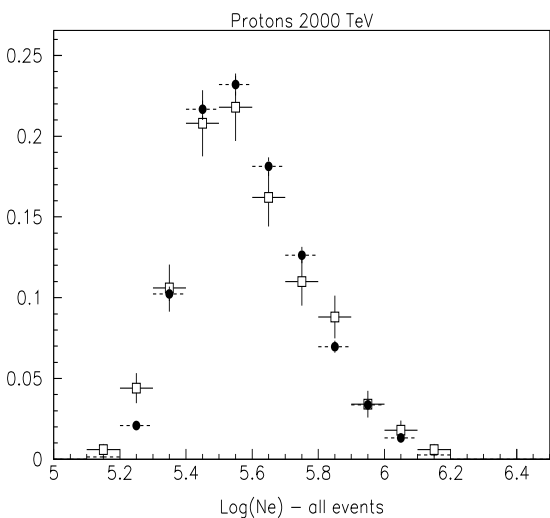


Figure 15. The distribution of the electron number at the sampling level calculated for 2000 TeV primary protons.

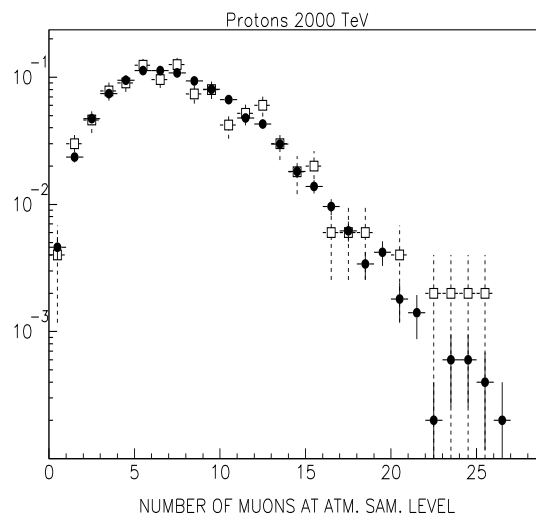


Figure 17. The multiplicity distribution of Muons at the sampling level

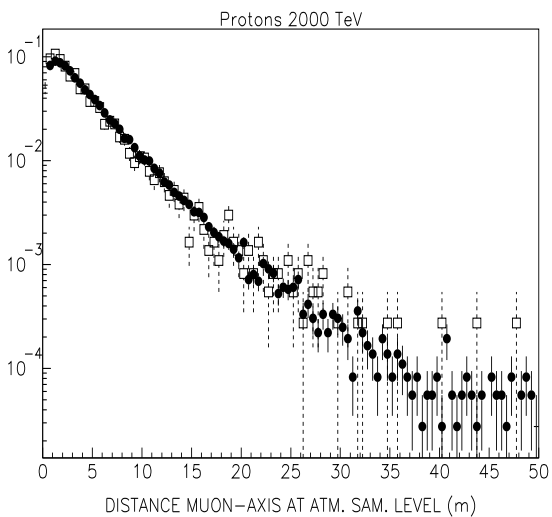


Figure 16. The distance muon-shower axis for  $E > 1$  TeV muons calculated for 2000 TeV primary protons. This distribution is mainly related to the transverse momentum distribution of pions and Kaons in the hadronic collisions.

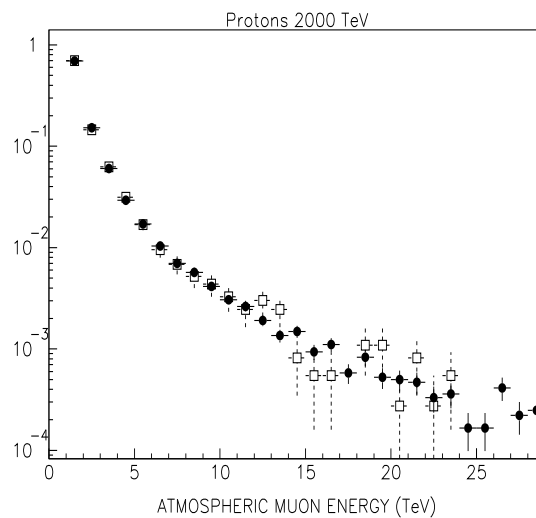


Figure 18. The energy spectrum of  $E > 1$  TeV muons at the sampling level.

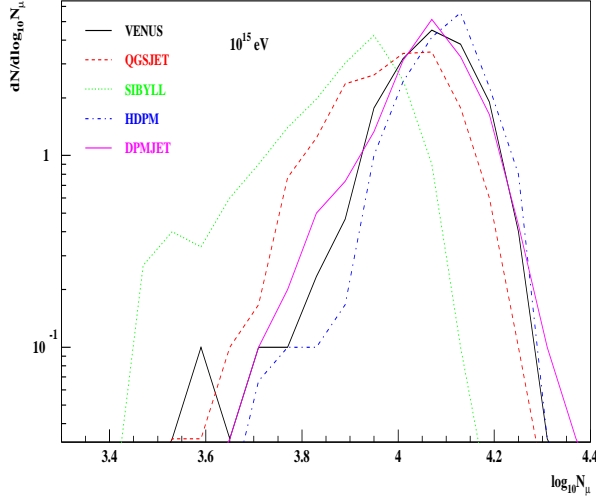


Figure 19. Muon number distribution at ground level from proton induced showers with  $E = 10^{15}$  eV. The distributions were calculated using the CORSIKA shower code [5] with 5 different event generators for the hadronic interactions.

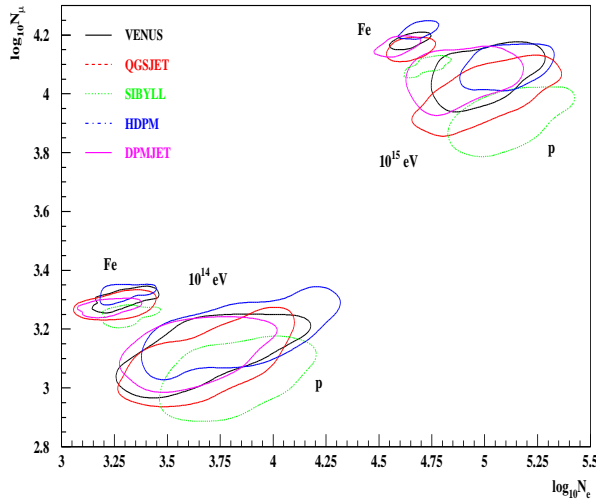


Figure 20. Contours in the  $\log_{10} N_{\mu} - \log_{10} N_e$  plane for p and Fe induced showers of  $E = 10^{14}$  and  $10^{15}$  eV .

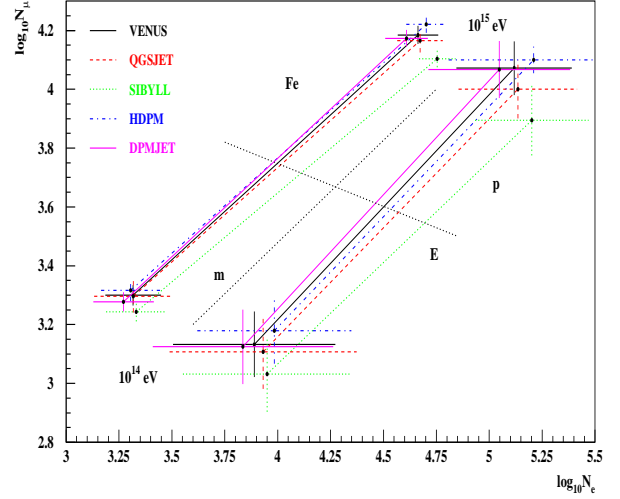


Figure 21.  $\log_{10} N_{\mu}$  over  $\log_{10} N_e$  for p and Fe induced showers of  $E = 10^{14}$  and  $10^{15}$  eV . Projecting along the lines (m) and (E) one can estimate the energy and mass of the primary.

- project design report, , Fermilab report, 1995
2. N. Chila and et al.: Nucl.Instr.Meth. A 311 (1992) 338
3. D. e. a. Bird: Proc. 23 nd ICRC (Calgary) 2 (1993) 38
4. P. Doll and et al.: The Karlsruhe cosmic ray project KASKADE, KFK 4686, Karlsruhe report, 1990
5. J. Knapp, D. Heck and G. Schatz: Comparison of hadronic interaction models used in Air shower simulations and their influence on shower development and observables, FZKA 5828, Karlsruhe report, 1996
6. J. Ranft: Phys. Rev. D 51 (1995) 64
7. J. Ranft: DPMJET-II, a Dual Parton Model event generator for hadron-hadron, hadron-nucleus and nucleus-nucleus collisions, Proceedings of the second SARE workshop at CERN, 1995, ed. by G.R.Stevenson, CERN/TIS-RP/977-05, p. 144., 1997
8. J. Ranft: DPMJET version II.3 and II.4, INFN/AE-97/45, Gran Sasso report, 1997
9. M. Glück, E. Reya and A. Vogt: Z. Phys.

- C67 (1995) 433
10. CTEQ-Collab.: H. L. Lai et al.: Phys. Rev. D55 (1997) 1280
  11. G. Battistoni, C. Forti and J. Ranft: Astroparticle Phys. 3 (1995) 157
  12. S. e. a. Ahlen: Nucl. Instr. Meth. A 324 (1993) 337
  13. R. S. Fletcher, T. K. Gaisser, P. Lipari and T. Stanev: Phys. Rev. D50 (1994) 5710
  14. E. Eichten and et al.: Rev. Mod. Phys. 56 (1984) 579
  15. J. Knapp and D. Heck: Extensive Air shower simulation with CORSIKA, KFK 5196 B, Karlsruhe report, 1993
  16. S. Ostapchenko, T. Thouw and K. Werner: Nucl. Phys. B 52B (1997) 3
  17. N. Kalmykov and et al.: Physics of Atomic Nuclei 58 (1995) 1728
  18. J. Capdevielle: J.Phys. G 15 (1989) 909
  19. A. Hillas: J.Phys.G 8 (1982) 1461;1475
  20. A. Capella, J. Tran Thanh Van and J. Kwiecinski: Phys. Rev. Lett. 58 (1987) 2015
  21. F. W. Bopp, A. Capella, J. Ranft and J. Tran Thanh Van: Z. Phys. C51 (1991) 99
  22. P. Aurenche, F. W. Bopp, A. Capella, J. Kwiecinski, M. Maire, J. Ranft and J. Tran Thanh Van: Phys. Rev. D45 (1992) 92
  23. R. Engel, F. W. Bopp, D. Pertermann and J. Ranft: Phys. Rev. D46 (1992) 5192
  24. K. Hahn and J. Ranft: Phys. Rev. D41 (1990) 1463
  25. F. W. Bopp, D. Pertermann, R. Engel and J. Ranft,: Phys. Rev. D 49 (1994) 3236
  26. A. D. Martin, R. G. Roberts and W. J. Stirling: Phys. Rev. D47 (1993) 867
  27. A. Donnachie and P. V. Landshoff: Phys. Lett. B296 (1993) 227
  28. G. Arnison et al.: Phys. Lett. B128 (1983) 336
  29. UA4 Collab.: M. Bozzo et al.: Phys. Lett. B147 (1984) 385
  30. N. A. Amos et al.: Nucl. Phys. B262 (1985) 689
  31. UA4 Collab.: D. Bernard et al.: Phys. Lett. B198 (1987) 583
  32. UA5 Collab.: G. J. Alner et al.: Z. Phys. C32 (1986) 153
  33. E710 Collab.: N. A. Amos et al.: Phys. Lett. B243 (1990) 158
  34. CDF Collab.: F. Abe et al.: FERMILAB-PUB-93/234-E, 1993
  35. CDF Collab.: F. Abe et al.: Phys. Rev. D50 (1994) 5518
  36. CDF Collab.: F. Abe et al.: Phys. Rev. D50 (1994) 5550
  37. H.H.Mielke, M.Föller, J.Engler and J.Knapp : J.Phys. G 20 (1994) 637
  38. UA5 Collab.: G. J. Alner et al.: Z. Phys. C33 (1986) 1
  39. CDF Collab.: F. Abe et al.: Phys. Rev. D41 (1990) 2330
  40. R. Harr and et al.: Pseudorapidity distribution of charged particles in  $\bar{p}p$  collisions at  $\sqrt{s} = 630$  GeV, Hep-ex/9703002, 1997
  41. NA22 Collab.: M. Adamus et al.: Z. Phys. C39 (1988) 311
  42. C. De Marzo et al.: Phys. Rev. D26 (1982) 1019
  43. NA35 Collaboration, presented by D.Röhrich at the QM93 Conference: Nucl. Phys. A 566 (1994) 35c
  44. CDF Collab.: F. Abe et al.: Phys. Rev. Lett. 77 (1996) 438
  45. G. Bocquet et al.: Phys. Lett. B366 (1996) 434
  46. UA1 Collab.: C. Albajar et al.: Nucl. Phys. B335 (1990) 261
  47. C. Forti, H. Bilokon, B. d'Ettorre Piazzoli, T.K. Gaisser, L. Satta and T. Stanev: Phys. Rev. D42 (1990) 3668
  48. M. Ambrosio, C. Aramo, G. Battistoni, C. Forti and J. Ranft: to be published, 1997
  49. Ferreiro, E.: these Proceedings, 1997